



# **13 TeV SUSY $\tilde{\tau}_1$ Search**

## **Estimation of Tau Fake Rate (TFR) in $\mu - \tau$ & $e - \tau$ Channels**

Emmanouil Vourliotis

National and Kapodistrian University of Athens

Supervisor: Alexis Kalogeropoulos (DESY)

DESY Summer Student Programme 2016  
07.09.16

### **Abstract**

Data accumulation from Run II of LHC has provided increased sensitivity for the 13 TeV SUSY search for  $\tilde{\tau}$ . The motivation of this project is to estimate the differences between simulation and data on the misidentification of jets which are reconstructed as taus. We apply the Tight-to-Loose method on a W+Jets pure sample in order to derive the appropriate scale factors to correct the Monte Carlo simulations.

# Contents

<b>1. Introduction</b>	<b>3</b>
<b>2. Theory</b>	<b>4</b>
2.1. The Signal of the Analysis . . . . .	4
2.2. $\tau$ decays . . . . .	5
2.3. Method . . . . .	6
<b>3. Analysis</b>	<b>7</b>
3.1. Datasets and Technical Details . . . . .	7
3.2. Preselection . . . . .	7
3.3. Loose/Tight ID and Tau Fake Rate . . . . .	8
3.4. Getting A High Purity W+Jets Sample . . . . .	9
3.5. Parametrization . . . . .	13
<b>4. Results</b>	<b>14</b>
4.1. Control Plots . . . . .	14
4.2. Tau Fake Rate and Scale Factors . . . . .	18
<b>5. Summary</b>	<b>20</b>
<b>A. Appendix: Datasets</b>	<b>22</b>
<b>B. Appendix: <math>e - \tau</math> Channel Control Plots</b>	<b>23</b>

# 1. Introduction

The Standard Model (SM) is a theory developed gradually during the 20th century and now comprises the fullest picture we have for the fundamental structure of the universe. In spite of its many successes, SM has left a number of unanswered questions:

1. *Dark Matter and Dark Energy*
2. *Hierarchy Problem*
3. *Large Number of Free Parameters*
4. *Grand Unified Theory*
5. *Quantum Gravity*
6. *Neutrino mass*
7. *Matter - Antimatter Asymmetry*

Supersymmetry (SUSY) is a theory that has been proposed as an extension to the SM, in order to cover some of its deficiencies. According to Supersymmetry (SUSY), every particle of the SM has a supersymmetric partner, which has every quantum number the same, except for its spin and mass. Taking into account that the difference in the spin of a particle is  $1/2$  and that this makes its spin from interger to half integer and vice versa, the spin-statistics theorem imposes that a fermion has a bosonic supersymmetric partner and a boson has a fermionic sypersymmetric partner. The Lightest Supersymmetric Particle (LSP) is neutral, weakly interacting and stable and is included in the final products of every supersymmetric decay. LSP is considered one of the major candidates for the explanation of Dark Matter.

SUSY in its simplest form predicts that every supersymmetric particle has the same mass as its SM counterpart. However, as there are currently no experimental evidence supporting SUSY, thus SUSY must a broken symmetry. A spontaneous symmetry breaking, similar with that of the Higgs Mechanism, would give the supersymmetric particles masses large enough to account for the fact that they have not been discovered in any experiment yet.

In many Supersymmetry models, one of the lightest particles is the supersymmetric partner of tau ( $\tau$ ), which is called stau ( $\tilde{\tau}$ ). As it is shown in figure 1, the cross section for the production of sleptons is much smaller than that of other supersymmetric processes. This is the reason why  $\tilde{\tau}$  production processes have been hardly investigated and only one point in the  $(M_{\tilde{\tau}}, M_{LSP})$  phase space has been excluded [5]. Our analysis is concentrated on stau production because the new data coming from LHC Run II RunII allows us to probe for these models given the increased sensitivity.

Any analysis that uses simulation samples needs to be corrected for effects not taken into account by simulations (e.g. triggering) or effects that are poorly described by simulations. An example in the latter case is the different rate at which a jet is misidentified



of staus via a chargino-chargino pair ( $\tilde{\chi}^\pm - \tilde{\chi}^\mp$ , middle figure) or chargino-neutralino pair ( $\tilde{\chi}^\pm - \tilde{\chi}^0$ , right figure). These production mechanisms give different final states, according to the decay mode of the taus produced. The different channels, along with their approximate branching ratios, are given in table 1.

Channel	Signature	$\mathcal{BR}$
$0 - \ell$	$\tau_h \tau_h$	$0.65^2 = 0.42$
$1 - \ell$	$\tau_\ell \tau_h$	$2 \times (0.35 \times 0.65) = 0.46$
$2 - \ell$	$\tau_\ell \tau_\ell$	$0.35^2 = 0.12$

Table 1: Stau analysis channels

In our analysis, we are concerned only with the semileptonic channel, that is with one tau decaying leptonically and the other decaying hadronically. These final states can be separated in two different channels, the ones in which the lepton is a muon ( $\mu - \tau$  channel) and the ones in which the lepton is an electron ( $e - \tau$  channel). We can see that this combination of channels has the highest branching ratio and it has a fairly clean signature, due to the existence of a lepton which we expect to be well isolated. Other characteristic experimental signatures are the small number of jets, the absence of b-jets and the fact that the Missing Transverse Energy (MET or  $\cancel{E}_T$ ) depends on the difference between the mass of the stau and the mass of the LSP, as the latter escapes detection and is thus reconstructed as MET.

## 2.2. $\tau$ decays

Tau is the heaviest of the leptons, with a mass of 1.78 GeV and a lifetime of  $2.9 \times 10^{-13}$  s. Apart from its decay to other leptons, its large mass makes it the only lepton that can decay hadronically (to pions). Due to the conservation of the leptonic number, every tau decay includes a tau neutrino in its final state. The different decay modes of the tau and their branching ratios are given in table 2.

Decay products of $\tau$	$\mathcal{BR}$
$e \bar{\nu}_e \nu_\tau$	17.85%
$\mu \bar{\nu}_\mu \nu_\tau$	17.36%
$Hadrons + \nu_\tau$	64.79%

Table 2: Tau Decays

Due to its short lifetime, a tau is never observed directly but its existence is inferred by the final products of its decay. Therefore, sophisticated algorithms [3] which combine a large number of variables are used to reconstruct and identify a tau based on the observed particles of an event. Although the reconstruction is relatively accurate for the leptonic decays, the hadronic decays are much more difficult to trace. Furthermore, the reconstruction in real Data and in Monte Carlo simulations are different. As a result,

the rate at which a jet is misidentified as a tau in Data is different than that in Monte Carlo simulations, leading to discrepancy between them. Therefore, the object of this report is to find and apply a method, in order to obtain the appropriate scale factors to make these rates equal and improve the description of the actual data in simulations.

### 2.3. Method

In order to estimate the tau fake rate, we have to find a sample that closely emulates the final state of our signal but has only jets and no taus. In this sample, we will count how many times a jet is misidentified as a tau in both Data and Monte Carlo. The best candidate sample to apply the method described above is W+Jets (figure 3a).

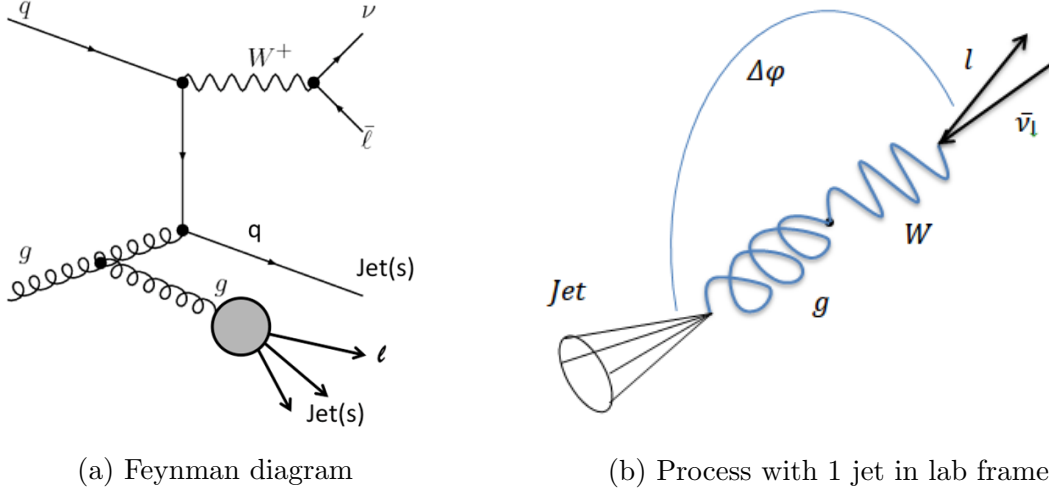


Figure 3: W+Jets

The W+Jets process is characterized by the production of a W boson and its decay into a lepton-neutrino pair and the existence of a number of jets which come from gluons or quarks. As an illustrated example, we take the case where we have only one jet (figure 3b). Then the prompt  $e$  or  $\mu$  will be well isolated, since it will be almost back-to-back with the jet, in the frame of reference in which the initial momentum is zero (lab frame). Due to the large Lorentz factor that the initial W is expected to have, the lepton and the neutrino are almost collinear with it and their momentums can be used to reconstruct the four-momentum of the W.

Even if we have more than one jet, then we can choose the events that have the above final state by requiring that there is a large separation between the jet and the W and that the transverse momentum of the jet is almost balanced by the transverse momentum of the W. In this way, we can also exclude other processes, e.g. semileptonic  $t\bar{t}$ , which may mimic the final state of our W+Jets sample.

### 3. Analysis

#### 3.1. Datasets and Technical Details

The Data we used corresponds to an integrated luminosity of  $15.9 \text{ fb}^{-1}$ . The trigger threshold for the muon is at 22 GeV and for the electron is at 25 GeV. The Data and Monte Carlo datasets used are shown in Appendix A.

#### 3.2. Preselection

The reconstruction and identification of physics objects follow official recommendations. The measurements of jets and MET make use of candidates reconstructed with the use of the particle flow (PF) algorithm ([6], [7]). The PF algorithm combines information from all subdetectors in order to identify leptons, photons as well as charged and neutral hadrons.

Before we give the preselection for our analysis, we define some kinematic variables. Pseudorapidity  $\eta$  is a measure for the polar angle of the trajectory of a particle. It is defined as  $\eta = -\ln \tan\left(\frac{\theta}{2}\right)$  and some values are shown in figure 4.  $d_{xy}$  &  $d_z$  are called impact parameter and measure the distance of the creation of a particle from the primary vertex in the transverse plane and along the z-axis respectively.  $R_{\text{ellso}}$  is the relative isolation that indicates if a particle is isolated from others. It is given by the sum of  $p_T$  of all other objects surrounding the object of interest within a cone of fixed  $\Delta R$  divided by the  $p_T$  of the object of interest.

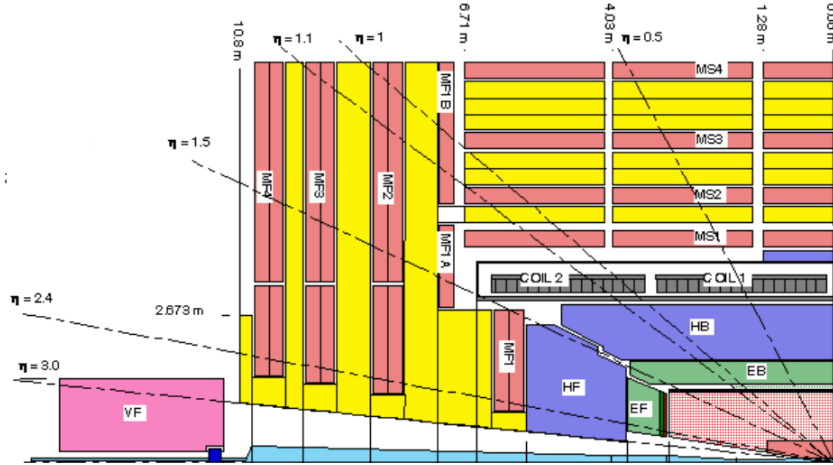


Figure 4: CMS Detector and  $\eta$  values

Below, we define the conditions that the detected objects should fulfil in order to be taken into account in our analysis. We begin with the definitions of the muon and the electron that are mainly dictated by the triggers we use, e.g. the  $p_T$  threshold is set about 1 GeV higher than the trigger in order to ensure maximum trigger efficiency. The preselection on  $\mu$  and  $e$  is shown in table 3.

	<b>Muon</b>	<b>Electron</b>
$P_T > (\text{GeV})$	23	26
$ \eta  <$	2.4	2.1
$d_{xy} < (\text{cm})$	0.045	0.045
$d_z < (\text{cm})$	0.2	0.2
$\text{RelIso} <$	0.15	0.1

Table 3: Lepton preselection

In the case that there are a few leptons that fulfil the above conditions, the highest  $p_T$ , most isolated lepton is selected. A similar procedure is applied for the identification of jets. The chosen jets (we require at least one jet) have to pass:

	<b>Jets</b>
$\text{pfLooseJets} >$	0
$P_T > (\text{GeV})$	20
$ \eta  <$	2.4
$\Delta R >$	0.5 (from lepton)

Table 4: Jets preselection

### 3.3. Loose/Tight ID and Tau Fake Rate

The main goal of this project is to calculate how many times a jet is misidentified as a tau. Therefore, we define two different IDs with which we tag our jets. The Loose ID is designed to count the tau jet candidates in our sample with opposite charge as the selected lepton and passing some loose tau ID discriminants (anti- $e$  and anti- $\mu$ ). The main selection criteria for the Loose ID are summarized in table 5.

	<b>Tau Candidate</b>
$P_T > (\text{GeV})$	20
$ \eta  <$	2.3
$d_z < (\text{cm})$	0.2

Table 5: Loose ID

The next step is to count how many of these jets are reconstructed as a tau by the tau identification algorithms. We define the Tight ID as the combination of the Loose ID together with the Tau ID [4]. We will use two different methods for the TauID: The MVA ID and the CutBased ID. After a jet has passed the Tight ID requirements, it will have been misidentified as a tau. The rate at which a purely hadronic jet has been misidentified as a tau is called Tau Fake Rate (TFR) and is given by the fraction:

$$TFR = \frac{TightID}{LooseID}$$



We compute the TFR for both Data and Monte Carlo and we anticipate that they are not equal due to different reconstruction of the taus in Data and Monte Carlo. In order to correct our Monte Carlo samples to account for this difference, we calculate the Tau Fake Rate Scale Factor (TFR SF) to be applied on the Monte Carlo:

$$TFR\ SF = \frac{TFR(Data)}{TFR(MC)} = \frac{\frac{TightID(Data)}{LooseID(Data)}}{\frac{TightID(MC)}{LooseID(MC)}}$$

### 3.4. Getting A High Purity W+Jets Sample

In addition to the preselection cuts, we also need to impose some cuts in order to ensure a high W+Jets purity in our sample, because this is the process we want to probe. We create some control plots of important kinematic variables just after preselection to check the agreement between Data and Monte Carlo. The variables we check are:

- $\cancel{E}_T$
- $M_T = \sqrt{2p_T(\ell)\cancel{p}_T(1 - \cos\Delta\phi(\ell, MET))}$
- $\Delta\phi(W, Jet)$
- $RatioSum = \frac{p_T(W) - p_T(Jet)}{p_T(W) + p_T(Jet)}$

In what is to follow, the W boson has been reconstructed using the lepton and  $MET$  four momentums, whereas "Jet" means the leading (highest  $p_T$ ) jet.

In the control plots below and throughout this report, we use the color code shown in figure 5. TTJets/singleT refer to events with a pair of  $t\bar{t}$  or a single  $t$ , whereas in TTX/TG the  $t$  is produced along with a massive boson or a photon. WJets is the sample of interest. DYJets refers to Drell-Yan processes and VV/VG/VVV includes production of two or three bosons.

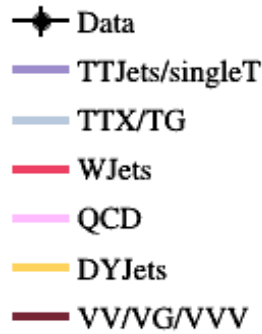


Figure 5: The color code for different processes

For simplicity and because we expect the distributions to be similar, we only give the control plots for the  $\mu$  channel:

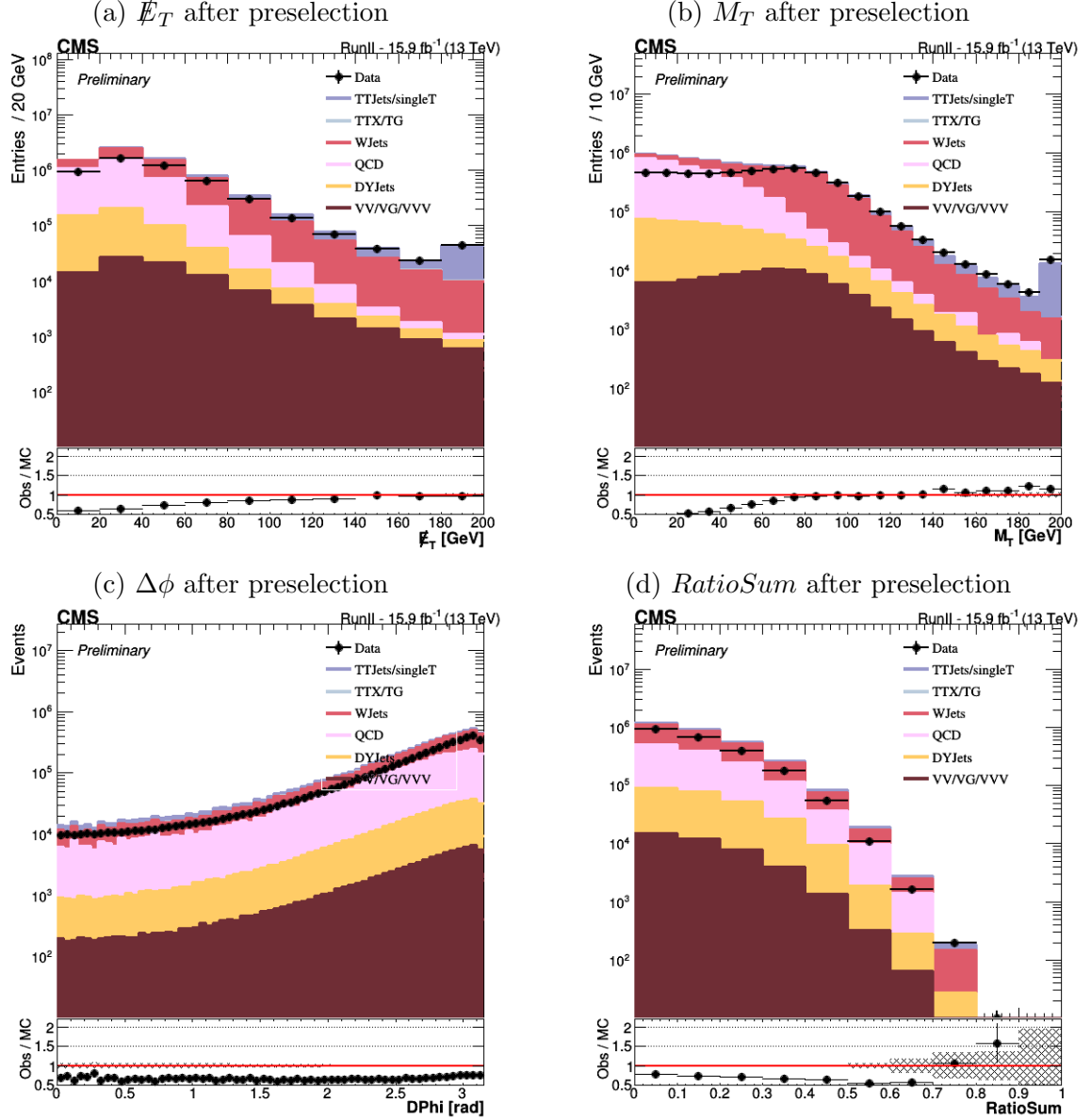


Figure 6: Control plots after preselection

First of all, it is evident that there is a significant disagreement between Data and Monte Carlo in some bins. However, we notice that this discrepancy is present mainly in bins where we have a lot of QCD (pink color). This is logical considering that we are using Monte Carlo QCD and that simulations cannot accurately reproduce actual QCD behaviour. Consequently, we have to impose such cuts so that most of QCD is excluded from our final selection. Keeping  $\cancel{E}_T$  over 40 or 60 GeV and  $M_T$  over 60 GeV seem like sensible choices. Apart from that, the  $t\bar{t}$  process is getting dominant in high  $\cancel{E}_T$  and  $M_T$ , so keeping events with  $M_T$  below 120 or 140 GeV seems that excludes most of it.

In order to quantify the above remarks, we check purity of our W+Jets sample:

$$Purity = \frac{\# \text{ of } W + \text{ Jets events}}{\# \text{ of all events}}$$

We calculate the *Purity* for the Loose and Tight collections and we find it to be 43% and 38% respectively, too low for the needs of the analysis. Then, we compute the *Purity* for each bin in all of the control variables (figure 7):

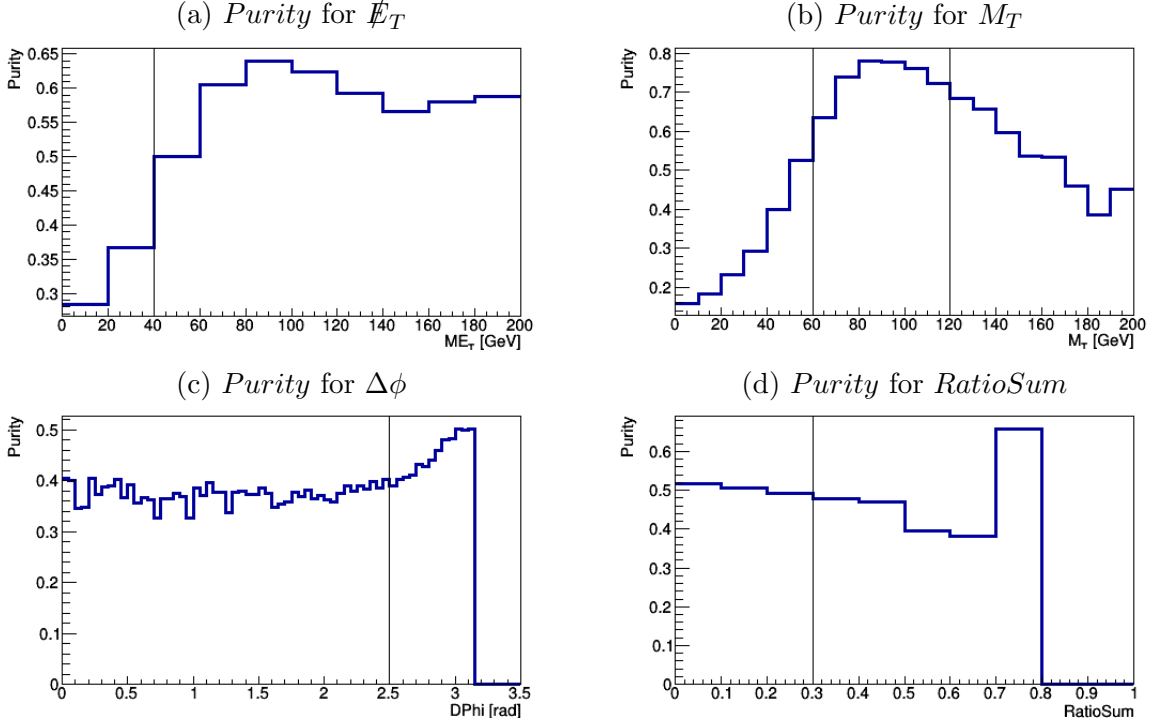


Figure 7: Purity per bin for the control variables

The vertical lines in figures 7a, 7b, 7c and 7d signify values where we could have a cut on our control variables in order to enhance the sample's W+Jets purity. The  $60 < M_T < 120$  GeV window cut is a logical choice, since we know that  $M_T$  has an endpoint at the mass of the W boson ( $\sim 83$  GeV), with a "tail" as a result of detector smearing due to limited resolution and reconstruction effects, for the W+Jets process. We would also like to exclude the  $\Delta\phi$  below 2.5, because W+Jets events have well separated Jet and lepton (figure 3b). According to the *Purity* plots, the cut in  $\cancel{E}_T$  and *RatioSum* should be around 40 GeV and 0.3 respectively.

We can check whether the cuts proposed above make sense by checking 2D plots to compare the behaviour of the W+Jets process and the rest of the processes (we name them "bkg") and see potential correlations in 2D purity plots (figures 8 and 9).

The figures 8a, 9a and 9b, 8b are the normalized plots showing the number of events (N) in each bin for the bkg and the W+Jets respectively, while figures 8c, 9c show the *Purity*. The 2D plots verify the appropriate points to apply cuts on our control variables

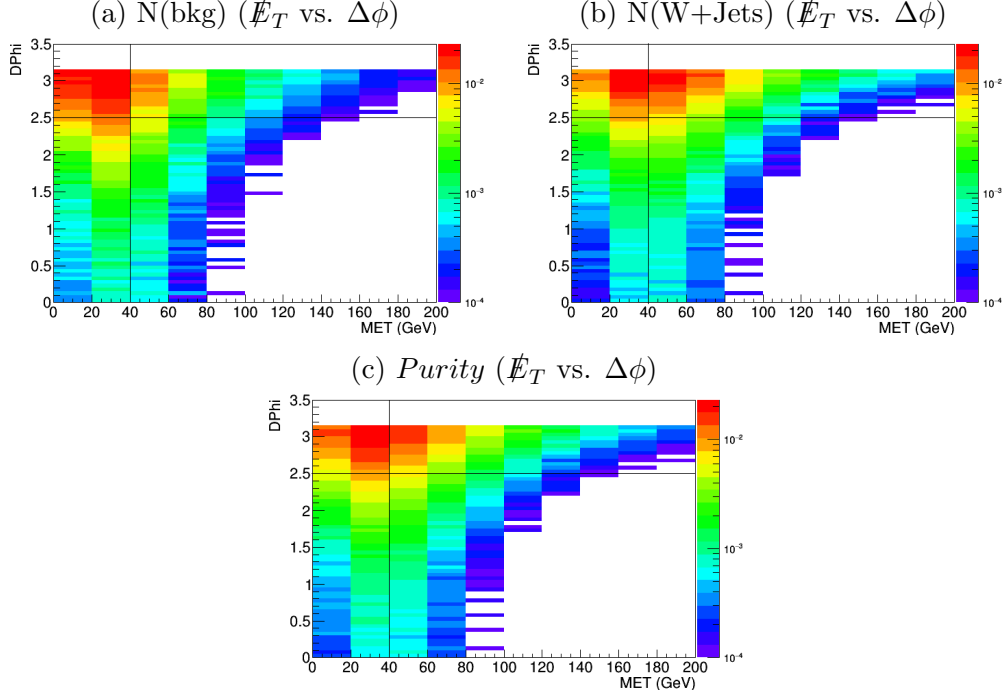


Figure 8:  $\cancel{E}_T$  vs.  $\Delta\phi$  2D plots

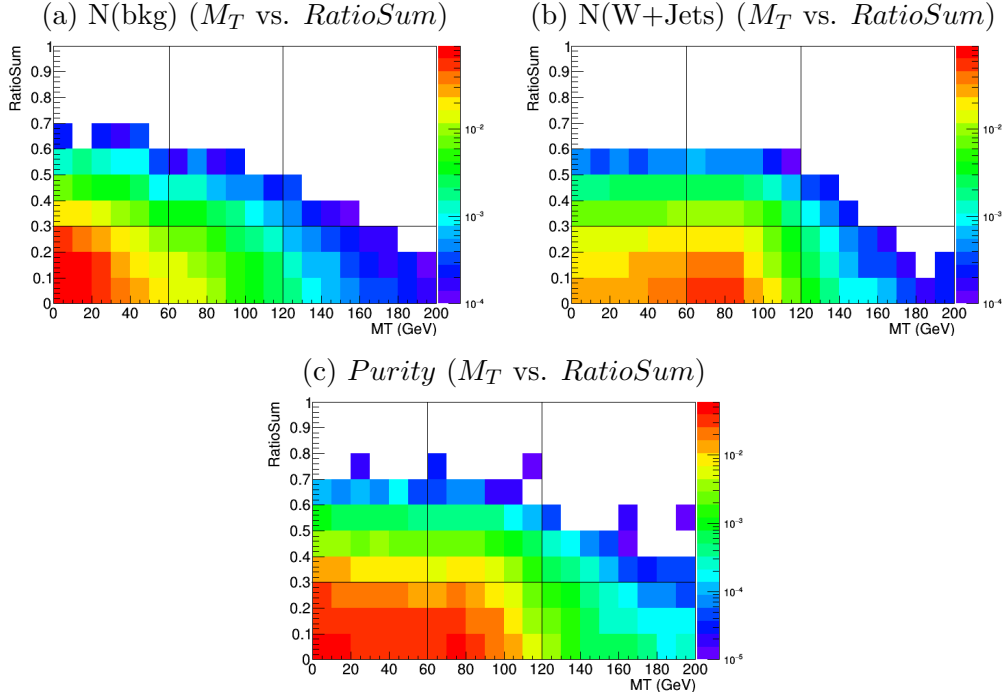


Figure 9:  $M_T$  vs.  $RatioSum$  2D plots

according to the distribution of number of events. We exclude the regions where we have a high concentration of bkg events and keep the regions where the number of W+Jets is high, taking into account the regions where *Purity* is maximized. We also exclude the regions where we have a lot of QCD, as shown in figure 6.

Below, we summarize the additional cuts (sequentially applied in the order presented) imposed in order to maximize the W+Jets purity:

- $\cancel{E}_T > 40 \text{ GeV}$
- $60 < M_T < 120 \text{ GeV}$
- $\Delta\phi(W, Jet) > 2.5$
- $RatioSum < 0.3$

After the application of these cuts, the *Purity* has almost doubled. The final *Purity* for the Loose collection has climbed to 82% (vs. 43% initially) and for Tight collection to 77% (vs. 38% initially).

### 3.5. Parametrization

The Tau Fake Rate is parametrized into  $(p_T(\tau), \eta(\tau))$  bins. The detector resolution is getting better at higher momenta, which means that tau reconstruction is also improving. Considering that TFR depends on the accuracy of tau reconstruction and identification, we expect that TFR changes with  $p_T(\tau)$  and it gets smaller as  $p_T(\tau)$  increases. In addition to that, we make the appropriate  $p_T(\tau)$  binning to ensure sufficient statistics in each bin. We have 3  $p_T(\tau)$  bins:

- $20 \text{ GeV} < P_T < 30 \text{ GeV}$
- $30 \text{ GeV} < P_T < 50 \text{ GeV}$
- $50 \text{ GeV} < P_T$

The  $\eta(\tau)$  binning is dictated by the detector geometry. Different detectors (e.g. muon barrel or muon endcap) have different efficiencies and we expect to see some impact by this effect on our results. Based on the above, we have 4  $\eta(\tau)$  bins for the  $\mu$  channel and 3 for the  $e$  channel:

#### $\mu - \tau$ channel

- $0 < |\eta| < 0.9$
- $0.9 < |\eta| < 1.2$
- $1.2 < |\eta| < 2.1$
- $2.1 < |\eta| < 2.4$

#### $e - \tau$ channel

- $0 < |\eta| < 1.48$
- $1.48 < |\eta| < 2.1$
- $2.1 < |\eta| < 2.4$

## 4. Results

### 4.1. Control Plots

After we have applied all the cuts, we create some control plots to check the agreement we have between Data and Monte Carlo. The control plots of  $\cancel{E}_T$ ,  $M_T$ ,  $\Delta\phi$  &  $RatioSum$  for both MVA ID and CutBased ID are shown in figures 10, 11, 12, 13. For simplicity, we only give the  $\mu - \tau$  control plots here and the  $e - \tau$  channel control plots are given in Appendix B.

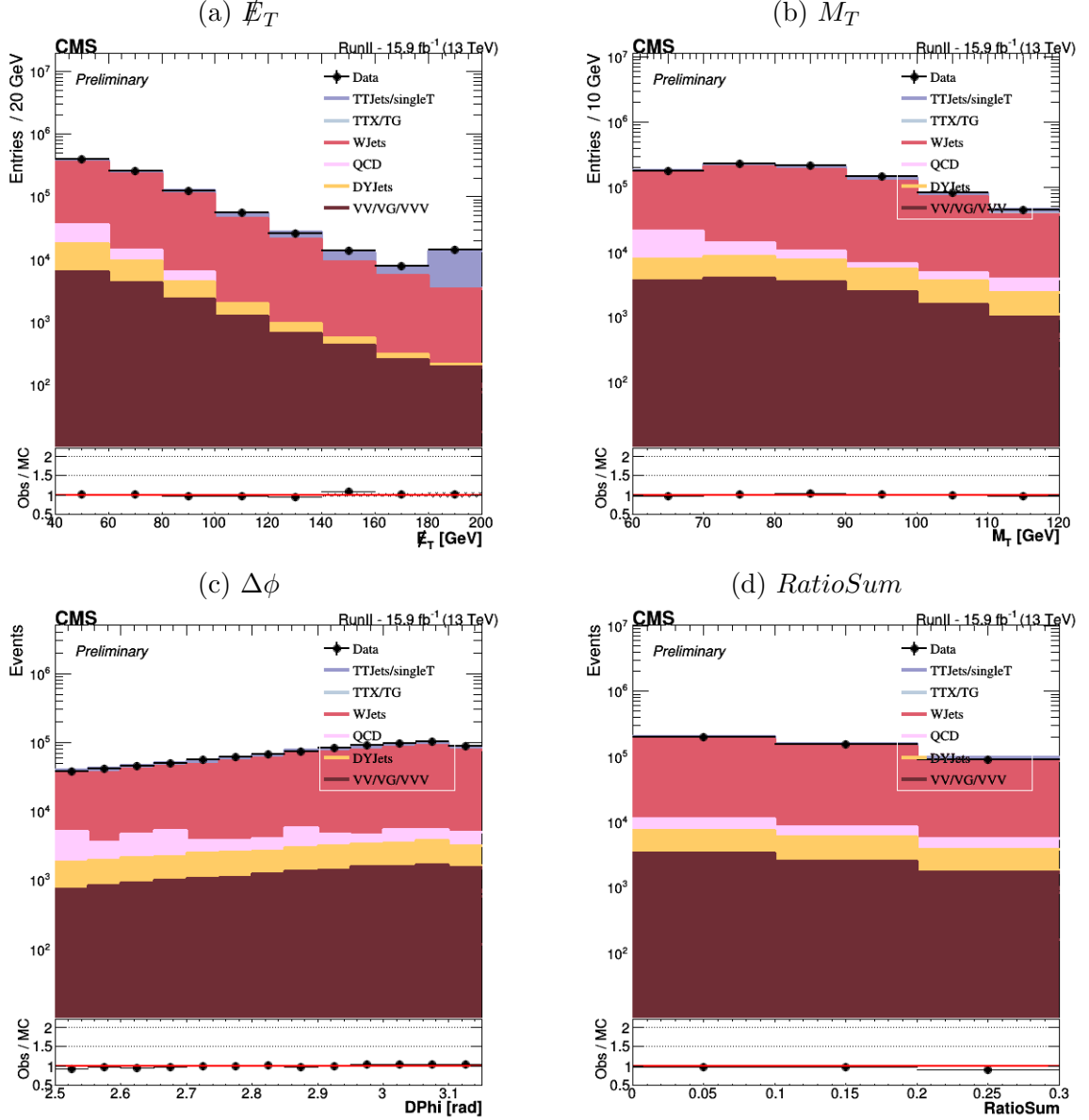


Figure 10:  $\mu - \tau$  channel MVA ID: Loose ID plots

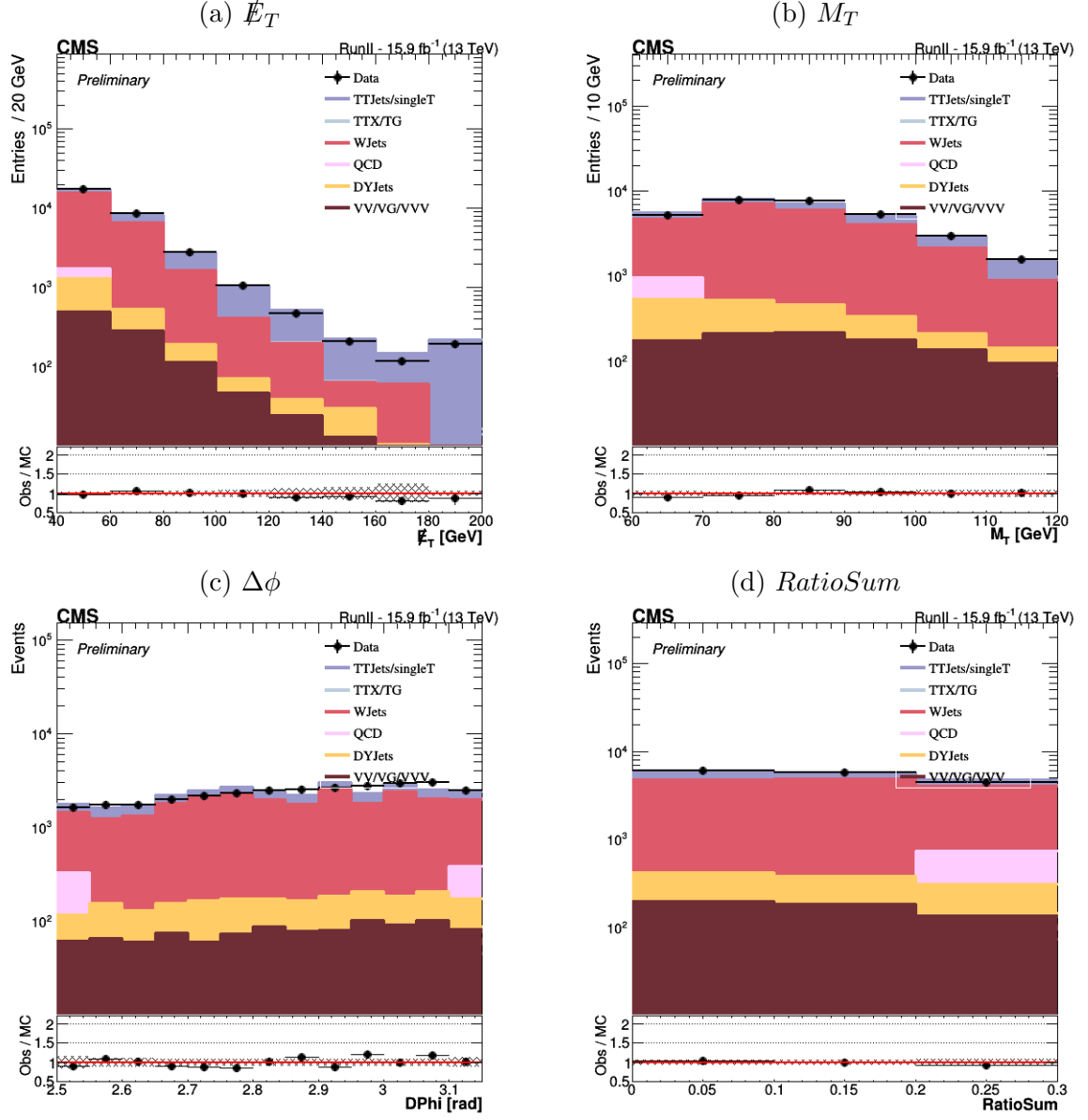


Figure 11:  $\mu - \tau$  channel MVA ID: Tight ID plots

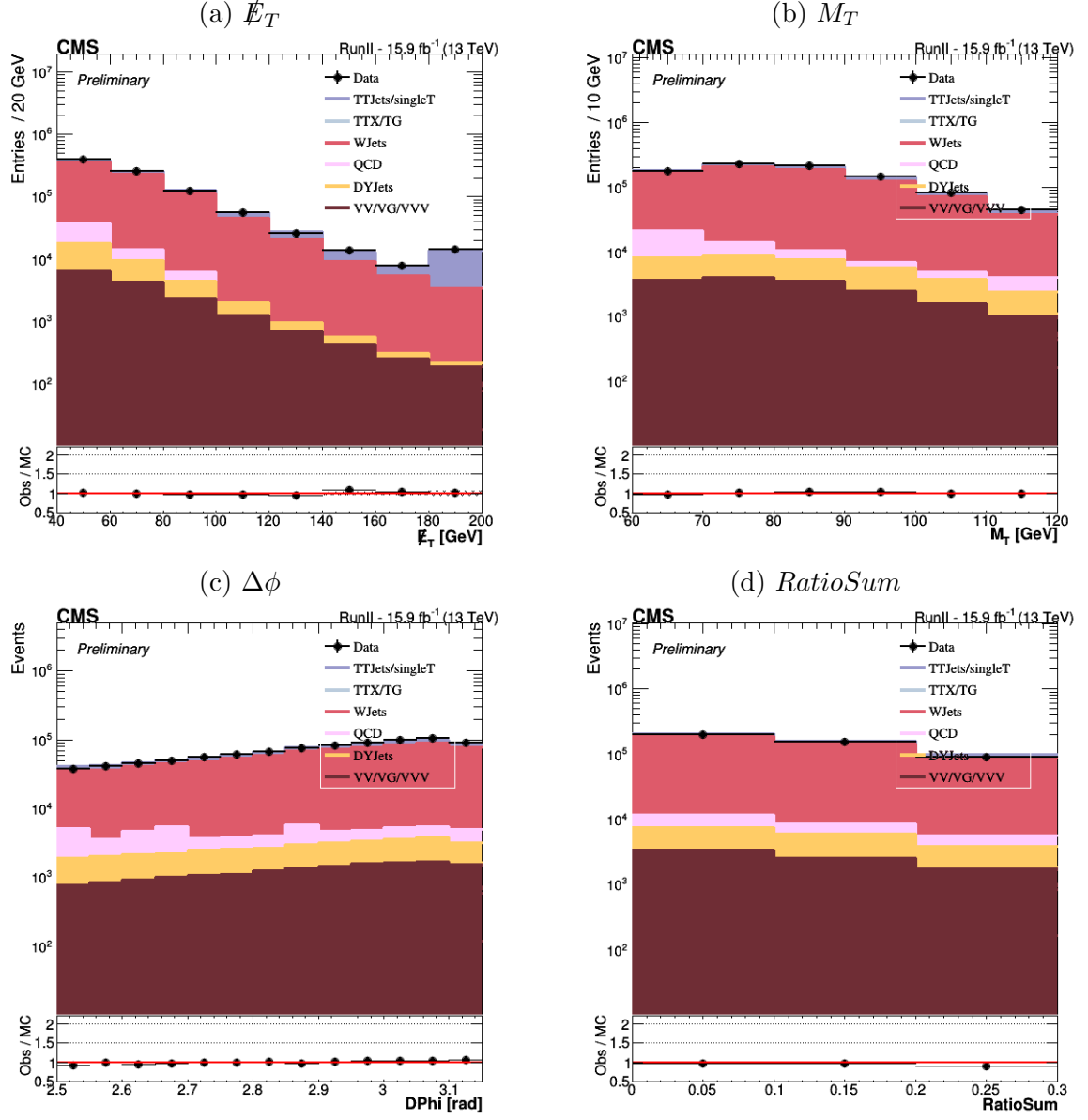


Figure 12:  $\mu - \tau$  channel CutBased ID: Loose ID plots



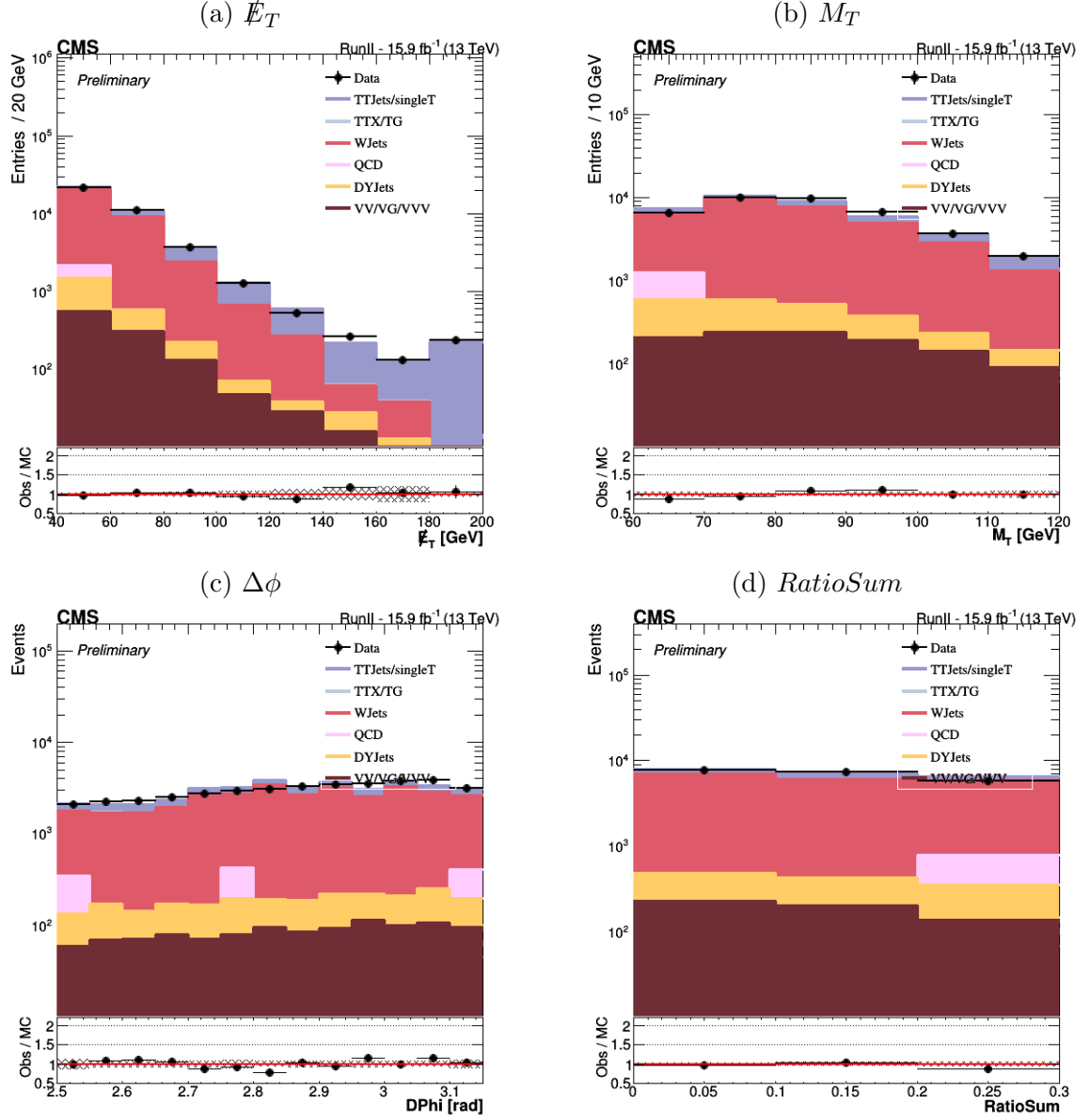


Figure 13:  $\mu - \tau$  channel CutBased ID: Tight ID plots

It is evident that our sample has a high W+Jets purity. Furthermore, we can see that our goal of eliminating QCD has succeeded. The presence of QCD in  $\mu - \tau$  channel is suppressed to below 10% and the same applies for the  $t\bar{t}$  process. The complete absence of QCD from the  $e - \tau$  channel is not real but an effect coming from the fact that we have limited statistics on the simulation sample. However, QCD is also suppressed to a minimum for that channel so that the above effect is insignificant. We also notice that the agreement is slightly better for the Loose ID than for the Tight ID and this demonstrates the need to introduce the TFR scale factors.

## 4.2. Tau Fake Rate and Scale Factors

Once we are sure that our sample is W+Jets pure and shows a good agreement between Data and Monte Carlo, we calculate the TFR for both Data and Monte Carlo. We do that by categorizing the events according to the  $p_T$  and  $\eta$  bins and then dividing the number of events that were tagged with the Tight ID by the number of events that were tagged with the Loose ID. Our results are presented in figures 14 and 15. We note that we use here a logarithmic x-axis.

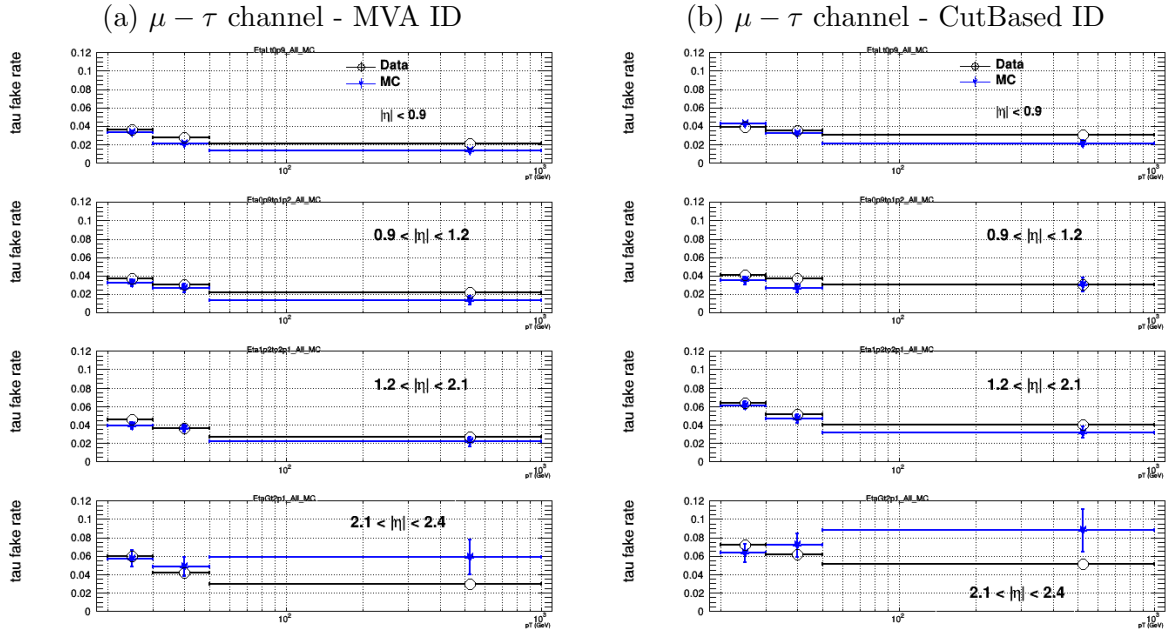


Figure 14: Tau Fake Rate plots for the  $\mu - \tau$  channel

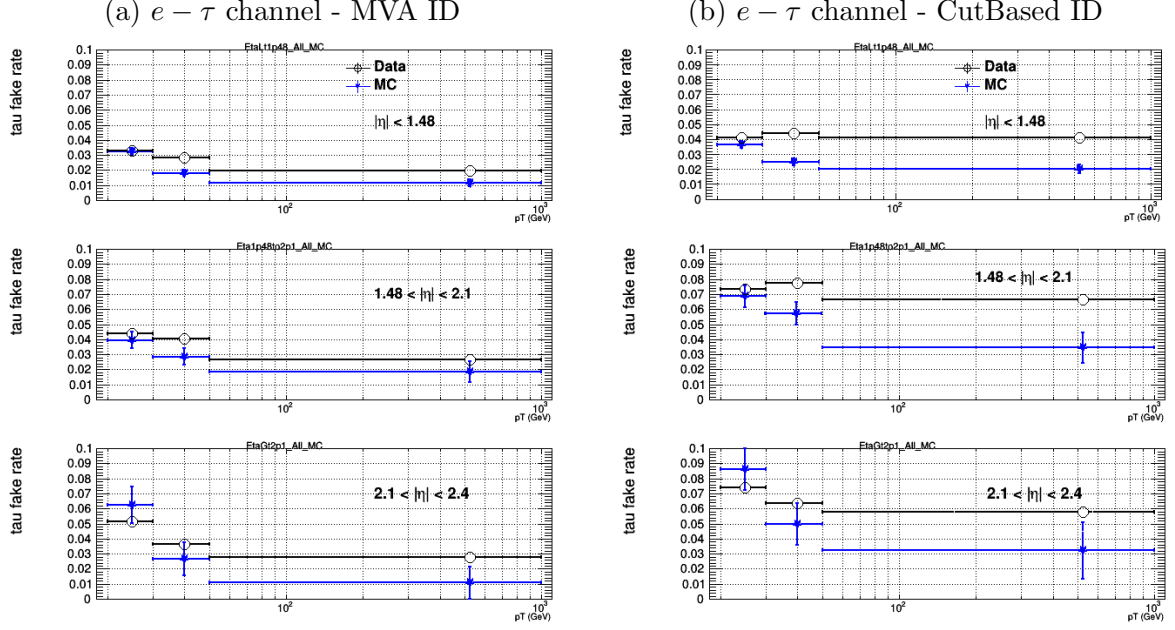


Figure 15: Tau Fake Rate plots for the  $e - \tau$  channel

The final step is to compute the Tau Fake Rate Scale Factors. The Scale Factors are just the division of the TFR for the Data by the TFR for the Monte Carlo, so we divide the values of the black points (Data) in figures 14 and 15 by the values of the blue points (MC) in the same plots. We also calculate the uncertainties, which are statistical only. The results for the TFR SF for the two channels and the two IDs are shown in tables 6, 7, 8 & 9.

MVA	$20 < P_T < 30\text{GeV}$	$30 < P_T < 50\text{GeV}$	$50\text{GeV} < P_T$
$0 < \eta < 0.9$	$1.07 \pm 0.07$	$1.30 \pm 0.13$	$1.5 \pm 0.3$
$0.9 < \eta < 1.2$	$1.13 \pm 0.14$	$1.16 \pm 0.20$	$1.7 \pm 0.6$
$1.2 < \eta < 2.1$	$1.16 \pm 0.10$	$1.00 \pm 0.11$	$1.22 \pm 0.29$
$2.1 < \eta < 2.4$	$1.04 \pm 0.17$	$0.86 \pm 0.18$	$0.51 \pm 0.16$

Table 6: Tau Fake Rate Scale Factors  $\mu - \tau$  channel - MVA ID

CutBased	$20 < P_T < 30\text{GeV}$	$30 < P_T < 50\text{GeV}$	$50\text{GeV} < P_T$
$0 < \eta < 0.9$	$0.92 \pm 0.05$	$1.07 \pm 0.09$	$1.45 \pm 0.22$
$0.9 < \eta < 1.2$	$1.17 \pm 0.14$	$1.39 \pm 0.23$	$1.02 \pm 0.25$
$1.2 < \eta < 2.1$	$1.05 \pm 0.07$	$1.11 \pm 0.10$	$1.27 \pm 0.24$
$2.1 < \eta < 2.4$	$1.14 \pm 0.17$	$0.86 \pm 0.15$	$0.58 \pm 0.16$

Table 7: Tau Fake Rate Scale Factors  $\mu - \tau$  channel - Cutbased ID

MVA	$20 < P_T < 30\text{GeV}$	$30 < P_T < 50\text{GeV}$	$50\text{GeV} < P_T$
$0 < \eta < 1.48$	$1.00 \pm 0.07$	$1.56 \pm 0.17$	$1.7 \pm 0.3$
$1.48 < \eta < 2.1$	$1.12 \pm 0.16$	$1.42 \pm 0.27$	$1.4 \pm 0.5$
$2.1 < \eta < 2.4$	$0.83 \pm 0.16$	$1.4 \pm 0.6$	$2.6 \pm 2.6$

Table 8: Tau Fake Rate Scale Factors  $e - \tau$  channel - MVA ID

CutBased	$20 < P_T < 30\text{GeV}$	$30 < P_T < 50\text{GeV}$	$50\text{GeV} < P_T$
$0 < \eta < 1.48$	$1.13 \pm 0.07$	$1.75 \pm 0.16$	$2.0 \pm 0.3$
$1.48 < \eta < 2.1$	$1.07 \pm 0.11$	$1.36 \pm 0.18$	$1.9 \pm 0.6$
$2.1 < \eta < 2.4$	$0.86 \pm 0.14$	$1.3 \pm 0.4$	$1.8 \pm 1.1$

Table 9: Tau Fake Rate Scale Factors  $e - \tau$  channel - Cutbased ID

We notice that most of the SF are close to unity. Most of the deviations of this trend occurs in the  $p_T > 50$  GeV bin, where the statistics are poor. The Cut Based ID seems to give a little bit larger differences from unity. As a whole, the MVA ID seems to be more robust and it the one that is used to correct the SUSY  $\tilde{\tau}$  search.

## 5. Summary

In this report, we have calculated the tau fake rate scale factors to be applied on simulations (integrated luminosity of  $15.9\text{fb}^{-1}$ ). First, we chose an appropriate sample (W+Jets) that can mimic the final state of our signal (direct and indirect stau search with semileptonic final state) but has no genuine taus. On this sample, we counted how many times a purely hadronic jets was misidentified as a tau in both Data and Monte Carlo. Then, we chose 4 variables and decided on the ideal cuts in order to maximize the W+Jets sample's purity. We applied the Tight-to-Loose method to extract the tau fake rate, parametrized in  $(p_T, \eta)$  bins, and we used the results to compute the corresponding scale factors that have to be applied to correct Monte Carlo samples. We have derived the results for both  $\mu - \tau$  and  $e - \tau$  channel and for both MVA and CutBased IDs. The results of this report can prove useful for other analyses involving hadronically decayed taus in the final state.

## References

- [1] <https://twiki.cern.ch/twiki/bin/view/CMSPublic/PhysicsResultsCombined>
- [2] <https://twiki.cern.ch/twiki/bin/view/LHCPhysics/SUSYCrossSections>
- [3] <https://twiki.cern.ch/twiki/bin/view/CMSPublic/SWGuidePFTauID>
- [4] CMS Collaboration, "Performance of reconstruction and identification of tau leptons in their decays to hadrons and tau neutrino in LHC Run-2", CMS-PAS-TAU-16-002 (2016).
- [5] G. Aad *et al.* [ATLAS Collaboration], "Search for the direct production of charginos, neutralinos and staus in final states with at least two hadronically decaying taus and missing transverse momentum in  $pp$  collisions at  $\sqrt{s} = 8$  TeV with the ATLAS detector", JHEP **1410** (2014) 096
- [6] CMS Collaboration, Particle-Flow Event Reconstruction in CMS and Performance for Jets, Taus, and Missing ET, CMS Physics Analysis Summary PFT-09-001 (2009).
- [7] CMS Collaboration, Commissioning of the Particle-Flow Reconstruction in Minimum-Bias and Jet Events from  $pp$  Collisions at 7 TeV, CMS Physics Analysis Summary PFT-10-002 (2010).

## A. Appendix: Datasets

MC Datasets
DYJetsToLL_M-10to50_TuneCUETP8M1_13TeV-madgraphMLM-pythia8
DYJetsToLL_M-50_TuneCUETP8M1_13TeV-madgraphMLM-pythia8
QCD_Pt-20toInf_MuEnrichedPt15_TuneCUETP8M1_13TeV-pythia8
WJetsToLNu_TuneCUETP8M1_13TeV-madgraphMLM-pythia8
ST_s-channel_4f_leptonDecays_13TeV-amcatnlo-pythia8_TuneCUETP8M1
ST_t-channel_antitop_4f_leptonDecays_13TeV-powheg-pythia8_TuneCUETP8M1
ST_t-channel_top_4f_leptonDecays_13TeV-powheg-pythia8_TuneCUETP8M1
ST_tW_antitop_5f_inclusiveDecays_13TeV-powheg-pythia8_TuneCUETP8M1
ST_tW_top_5f_inclusiveDecays_13TeV-powheg-pythia8_TuneCUETP8M1
TT_TuneCUETP8M1_13TeV-powheg-pythia8_ext4-v1
TGJets_TuneCUETP8M1_13TeV-amcatnlo-madspin-pythia8
TTGJets_TuneCUETP8M1_13TeV-amcatnloFXFX-madspin-pythia8
TTTT_TuneCUETP8M1_13TeV-amcatnlo-pythia8
tZq_ll_4f_13TeV-amcatnlo-pythia8
ttWJets_13TeV-madgraphMLM
ttZJets_13TeV-madgraphMLM
WWTo2L2Nu_13TeV-powheg
WWTo4Q_13TeV-powheg
WWToLNuQQ_13TeV-powheg
WW_DoubleScattering_13TeV-pythia8
WZTo1L1Nu2Q_13TeV-amcatnloFXFX-madspin-pythia8
WZTo1L3Nu_13TeV-amcatnloFXFX-madspin-pythia8
WZTo2L2Q_13TeV-amcatnloFXFX-madspin-pythia8
WZTo3LNu_TuneCUETP8M1_13TeV-powheg-pythia8
WGToLNuG_TuneCUETP8M1_13TeV-madgraphMLM-pythia8
WWG_TuneCUETP8M1_13TeV-amcatnlo-pythia8
ZGTo2LG_TuneCUETP8M1_13TeV-amcatnloFXFX-pythia8
ZGGJets_ZToHadOrNu_5f_LO-madgraph-pythia8
ZZTo2L2Nu_13TeV-powheg-pythia8
ZZTo2L2Q_13TeV-amcatnloFXFX-madspin-pythia8
ZZTo2Q2Nu_13TeV-amcatnloFXFX-madspin-pythia8
ZZTo4L_13TeV-powheg-pythia8
ZZTo4Q_13TeV-amcatnloFXFX-madspin-pythia8
WWW_4F_TuneCUETP8M1_13TeV-amcatnlo-pythia8
WWZ_TuneCUETP8M1_13TeV-amcatnlo-pythia8
WW_TuneCUETP8M1_13TeV-pythia8
WZZ_TuneCUETP8M1_13TeV-amcatnlo-pythia8
WZ_TuneCUETP8M1_13TeV-pythia8
ZZZ_TuneCUETP8M1_13TeV-amcatnlo-pythia8

Table 10: Monte Carlo Datasets

$\mu$ Data Datasets	e Data Datasets
Single_Muon_Run2016B_PromptReco_v2	Single_Electron_Run2016B_PromptReco_v2
Single_Muon_Run2016C_PromptReco_v2	Single_Electron_Run2016C_PromptReco_v2
Single_Muon_Run2016D_PromptReco_v2	Single_Electron_Run2016D_PromptReco_v2
Single_Muon_Run2016E_PromptReco_v2	Single_Electron_Run2016E_PromptReco_v2

Table 11: Data Datasets

## B. Appendix: $e - \tau$ Channel Control Plots

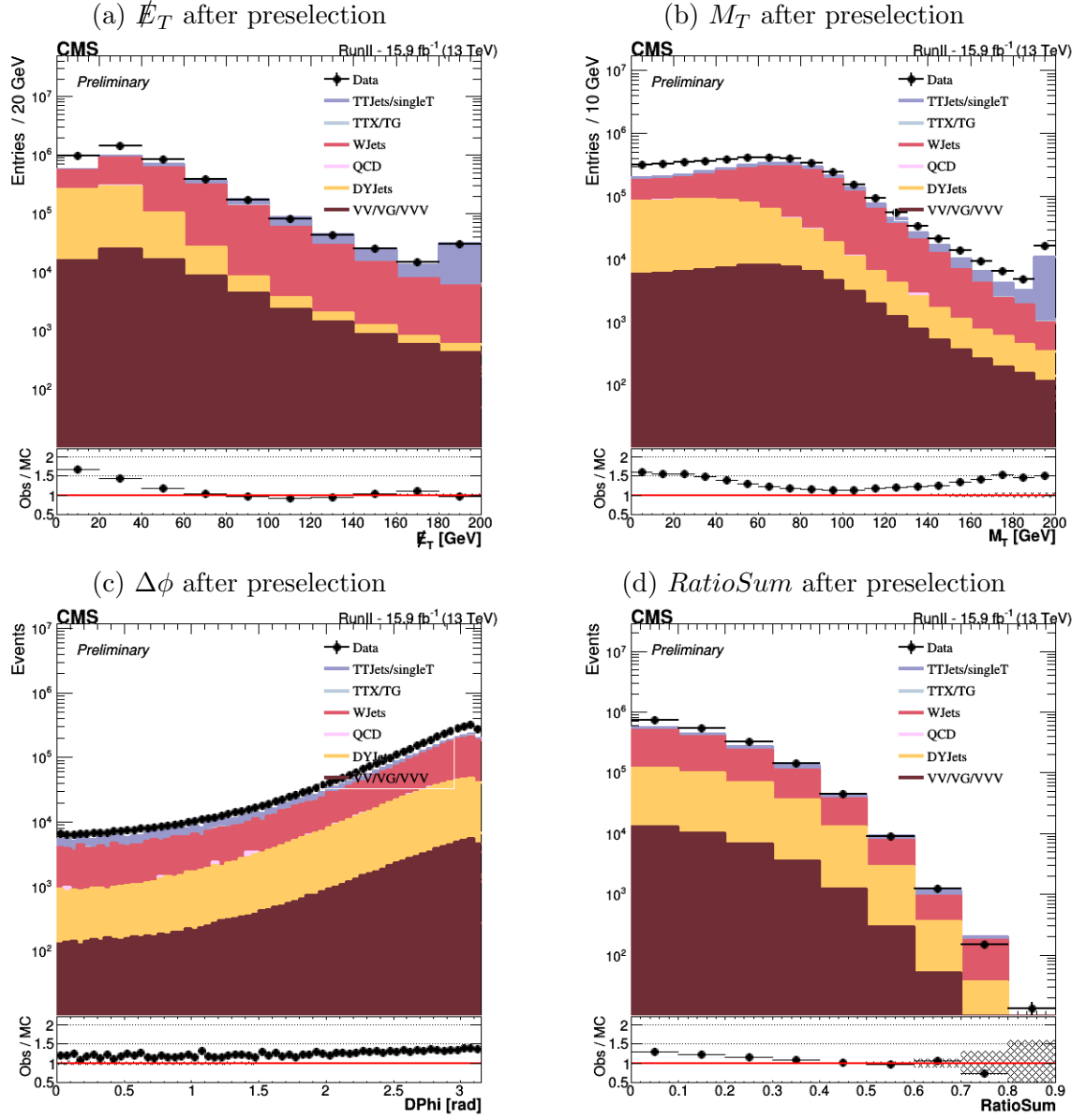


Figure 16: Control plots after preselection

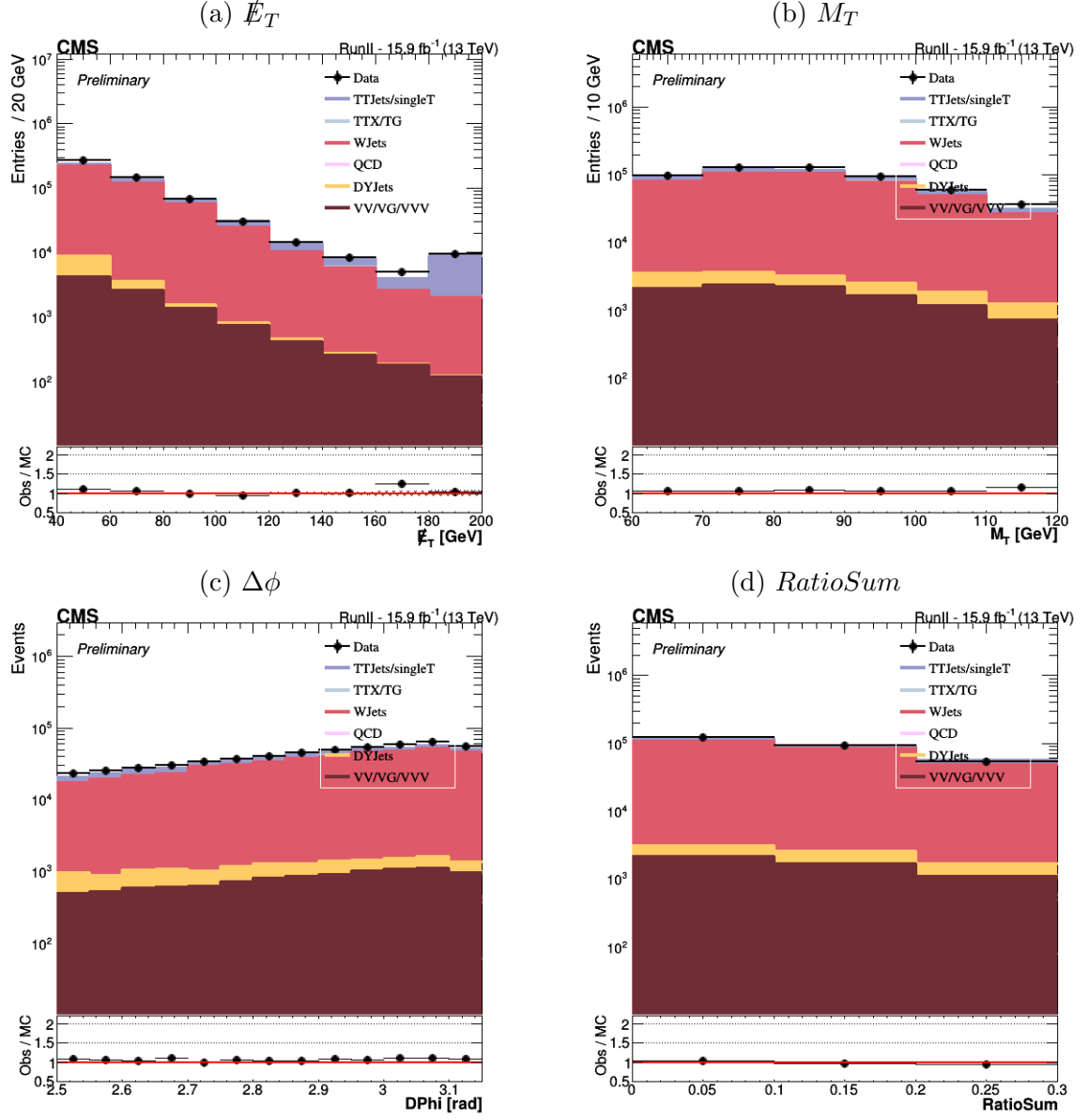


Figure 17:  $e - \tau$  channel MVA ID: Loose ID plots



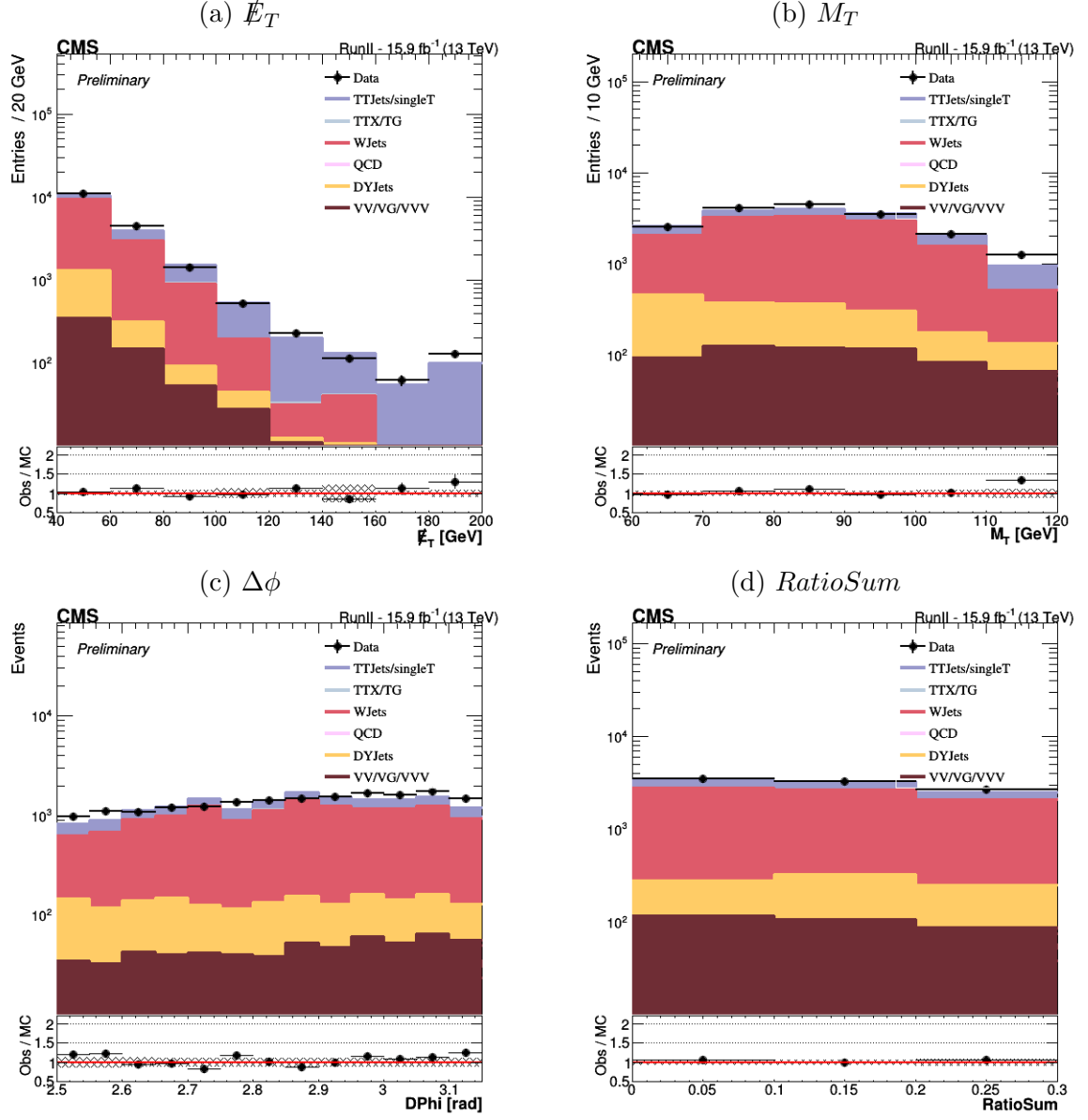


Figure 18:  $e - \tau$  channel MVA ID: Tight ID plots

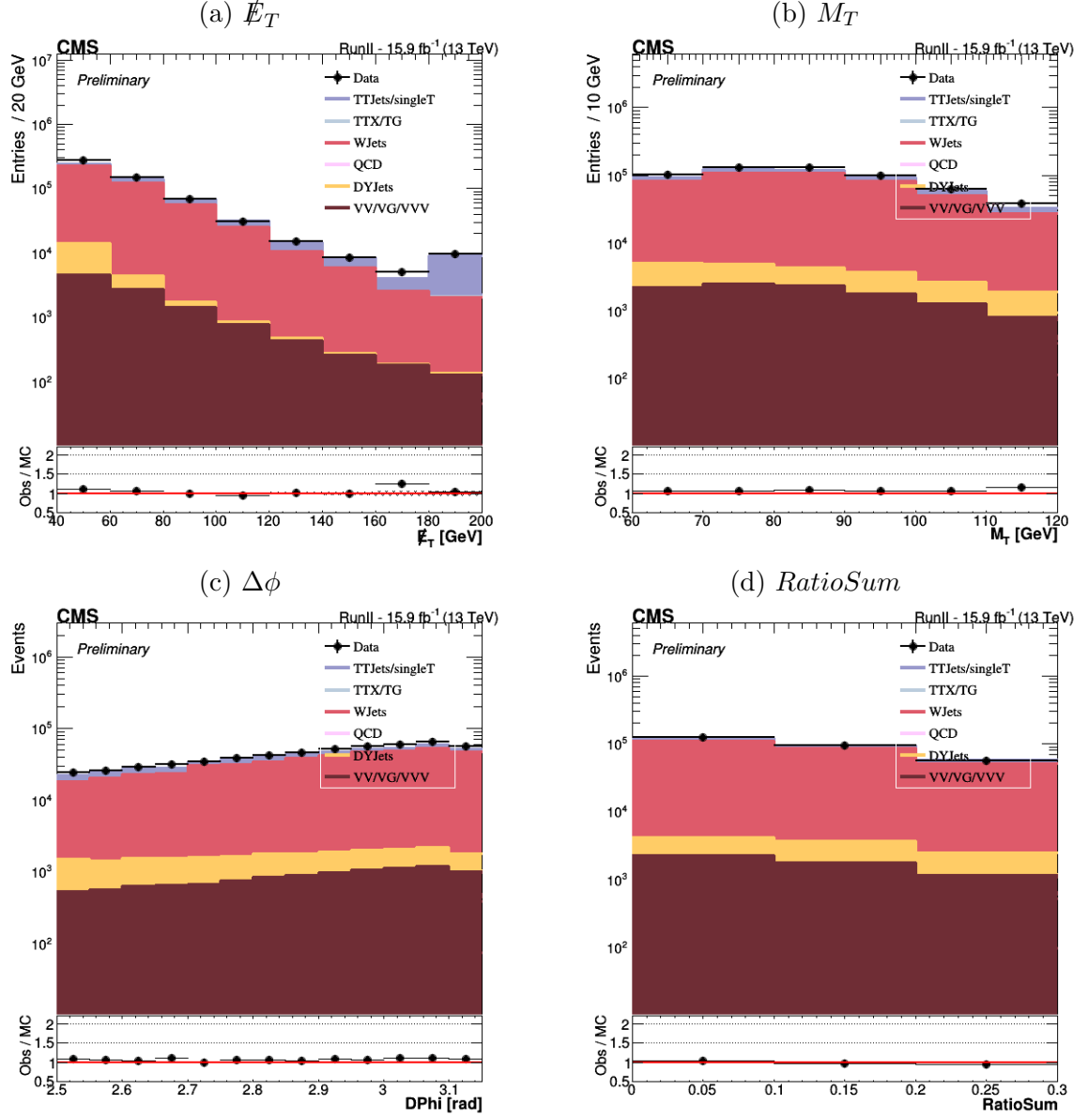


Figure 19:  $e - \tau$  channel CutBased ID: Loose ID plots

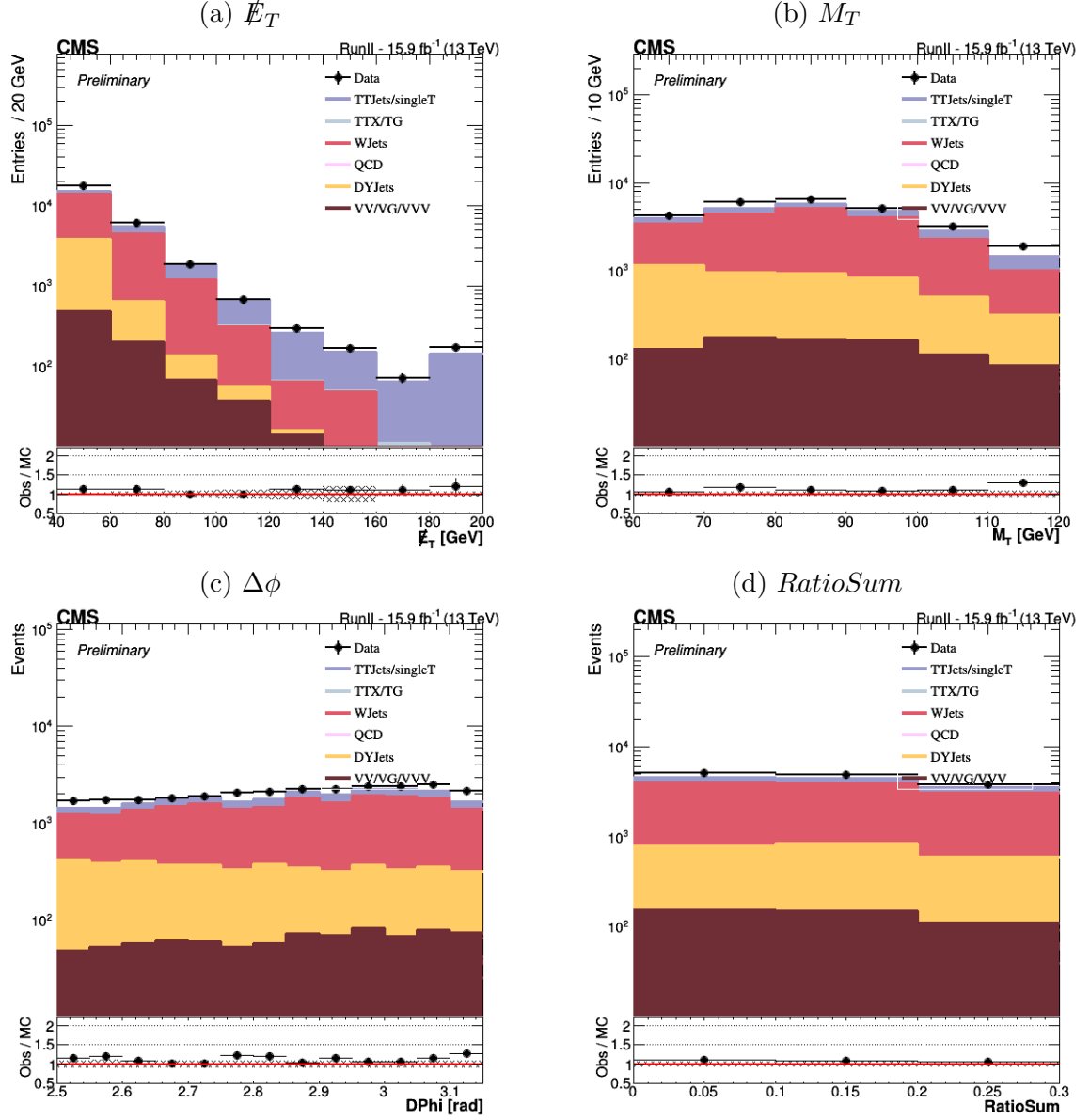


Figure 20:  $e - \tau$  channel CutBased ID: Tight ID plots